# Experimental Study of a Three-Dimensional, Shear-Driven, Turbulent Boundary Layer

David M. Driver* and Sheshagiri K. Hebbar†
*NASA Ames Research Center, Moffett Field, California*

**Experimental data have been obtained in a three-dimensional, shear-driven, turbulent boundary layer subjected to sudden transverse strain. Measurements made with a newly developed, three-component, laser Doppler velocimeter include all components of mean flow, turbulent Reynolds stresses, and triple-product correlations. Eddy viscosities, production, convection, turbulent diffusion, and dissipation (balance of kinetic energy equation) are extracted from the data. It is shown experimentally that eddy viscosity is strongly direction-dependent (not a scalar), indicating a need for full Reynolds stress modeling. Turbulence models for eddy viscosity, stress diffusion, pressure rate-of-strain, and anisotropy of Reynolds stresses are tested using the data. Calculations using a Reynolds stress equation model compared favorably with the data.**

## Nomenclature

$C_{fx}$ = wall skin-friction coefficient in the $x$ direction, $= \tau_{wx}/\frac{1}{2}\rho U_{\text{ref}}^2$
$C_{fz}$ = wall skin-friction coefficient in the $z$ direction, $= \tau_{wz}/\frac{1}{2}\rho U_{\text{ref}}^2$
$k$ = turbulent kinetic energy
$Q$ = resultant velocity vector
$r$ = radial distance from cylinder centerline
$R_0$ = radius of cylindrical model
$U, V, W$ = mean velocities in the $x$, $r$, and $\theta$ directions, respectively
$U_e$ = mean axial velocity at the edge of the boundary layer
$\overline{u^2}, \overline{v^2}, \overline{w^2}$ = mean-square velocity fluctuations in the $x$, $r$, and $\theta$ directions, respectively
$\overline{uv}, \overline{vw}, \overline{uw}$ = mean-square velocity fluctuation correlations
$\overline{vk}$ = turbulent, triple-product correlation of $k$ with $v$ fluctuations
$\overline{v^2 w}$ = turbulent triple-product correlation of $vw$ with $v$
$W_s$ = transverse velocity on the surface of the rotating cylinder
$X$ = axial distance measured from the junction of spinning and nonspinning sections
$Y$ = distance normal to the cylinder's surface, radial direction
$Z$ = tangential distance, circumferential direction
$\beta$ = skew angle of horizontal velocity vector relative to the freestream
$\delta$ = boundary-layer thickness
$\epsilon$ = dissipation rate of kinetic energy
$\nu$ = molecular kinematic viscosity
$\nu_t$ = eddy viscosity
$\tau_{wx}$ = surface shear stress along axis of cylinder
$\tau_{wz}$ = surface shear stress in transverse direction
$\omega$ = specific dissipation rate of turbulence kinetic energy, $\epsilon/(0.09k)$

*Superscripts*

$(\bar{\ })$ = long time average

*Subscripts*

$x$ = $X$ direction
$z$ = $Z$ direction
0 = reference location, $X = 0$

Presented as Paper 85-1610 at the AIAA 18th Fluid Dynamics, Plasmadynamics and Lasers Conference, Cincinnati, OH, July 16-18, 1985; received July 26, 1985; revision received May 19, 1986. 

*Research Scientist.
†Senior NRC Research Associate; currently at Tuskegee University, Tuskegee, AL.

## Introduction

SUCCESSFUL aerodynamic simulations of flight vehicles requires careful treatment of the turbulence generated along the vehicle surfaces. Faulty simulation of the turbulence can produce inaccurate predictions of drag, stall characteristics, shock location, etc. Simulations that solve for all small-scale motions of turbulence require prohibitively large computational memories and times. Alternatively, turbulence models can be used to simplify the computation while capturing the important flow physics necessary for engineering accuracy. Useful turbulence models are being developed to describe a wide range of two-dimensional flows. Expecting a turbulence model developed for two-dimensional flow to adequately describe a three-dimensional flow may be unreasonable. In contrast, relatively little work has been done on three-dimensional turbulence modeling.[1] Well-planned experiments using new instrumentation are needed to guide such an effort.

In practice, three-dimensional flows usually arise from transverse pressure gradients, such as those that occur on swept wings, rotating turbines, or in curved ducts. Likewise, most experiments[2-4] utilize transverse pressure gradients to generate a crossflow, making it difficult to study viscous effects independently.

An innovative experiment was devised by Furuya[5] et al. to study a three-dimensional boundary layer without pressure gradients. They studied the growth of crossflow produced by a spinning cylinder aligned with a uniform flow. Bissonnette and Mellor[6] and Lohmann[7] later reported turbulence measurements on similar experiments, suggesting that turbulent shear stresses may not be simply proportional to the mean flow strain (via scalar eddy viscosity) as is often assumed. Instead, eddy viscosity appeared to be anisotropic [i.e., $-\overline{uv}/(\partial U/\partial y) = -\overline{vw}/(\partial W/\partial r - W/r)$]. A further experimental and computational study was performed by Higuchi and Rubesin,[8,9] in which they studied the decay of

crossflow on a stationary section of cylinder immediately downstream of a spinning section. In their computational study, they showed that models which accounted for anisotropy of eddy viscosity predicted crossflow better than those that used scalar eddy viscosity. However, sizable discrepancies remained between the measurements and calculations, which were thought to be caused by the pressure rate-of-strain model. They were able to make direct measurements of skin friction in an effort to find a law of the wall in three-dimensional flow. Mean flowfield measurments were reported, but no turbulence measurements were obtained. A review of spinning cylinder flows is given by Nakamura and Yamashita.[10]

This paper presents flowfield measurements in a relaxing three-dimensional boundary layer, a continuation of the work presented by Higuchi and Rubesin.[8] A newly developed three-component laser Doppler velocimeter (LDV) has been used to measure three components of mean velocity, all six Reynolds stresses, and ten triple products. Eddy viscosities, turbulent production, convection, diffusion, dissipation (balance of kinetic-energy equation), and pressure strain (balance-of-stress equation) are extracted from the data. Turbulence models for eddy viscosity, stress diffusion, pressure rate of strain, and anisotropy of Reynolds stresses are tested using the data. Calculations using a Reynolds stress equation model are compared with the data. These new data, along with measured values of skin friction, have proven useful in clarifying turbulence modeling questions.

## Experiment

### Test Configuration

The experiment was conducted using the same apparatus as Higuchi and Rubesin[8]: a $0.31 \times 0.31$-m low-speed wind tunnel with a 0.140-m cylinder running the length fo the tunnel along its centerline (Fig. 1). The tunnel walls were deflected to produce a zero-pressure gradient along the cylinder. The upstream section of the cylinder (0.914 m long) was made to rotate with a circumferential speed equal to that of the freestream. The downstream section remained stationary. The gap between the spinning and stationary sections was closed to within 0.254 mm. The spinning and stationary cylinders were equal in diameter (0.140 m) to within $\pm 0.2$ mm (the upstream spinning cylinder was slightly smaller in diameter, 0.2 mm, than the stationary section). Measurements were taken primarily on the stationary section where the flow was relaxing from a three-dimensional boundary layer back to a two-dimensional boundary layer.

The experiment was performed at a freestream velocity of 36 m/s and atmospheric pressure and temperature. The boundary-layer thickness at the end of the spinning section was 0.025 m at a Reynolds number (based on momentum thickness) of 6000.

### Surface and Flowfield Measurements

Surface skin friction was measured using a fence gage developed by Higuchi and Rubesin.[8] Uncertainties in the skin-friction coefficient $C_f$ were estimated to be $\pm 10\%$ of the measured value.

Flowfield measurements were made using a three-component, synchronous, three-color LDV (see Appendix for details). Simultaneous measurements of each of three velocity components were used to construct time-averaged mean velocities, Reynolds stresses, and triple products. Uncertainties in $\underline{U}$, $\underline{V}$, and $\underline{W}$ were estimated to be $\pm 2\%$. Uncertainties in $\underline{u^2}$, $\underline{v^2}$, and $\underline{w^2}$ were estimated to be $\pm 7\%$. Uncertainties in $\underline{uv}$, $\underline{vw}$, and $\underline{uw}$ were estimated to fall in the range $-7$ to $+20\%$. The weighted uncertainty reflects the general belief that measured shear stresses are systematically lower by 10–20% than the actual values as a result of multiple seed particle measurements (see Appendix and Ref. 11 for discussion). Triple-product correlations (i.e., $\underline{vk}$) are also expected to be measured low by 10–20%, and uncertainties are estimated to be $-20$ to $+30\%$. Difficulties resulting from multiple seed particles do not affect the mean-velocity or kinetic-energy measurements.

### Flowfield Quality

Balance of the momentum integral equations was done to check the overall quality of the flowfield and self-consistency of the measurements. Changes in streamwise and transverse momentum were equal to streamwise and transverse skin-friction forces to within $\pm 7\%$, indicating a high level of self-consistency of the data and good axisymmetry of the flow.

## Computations

Computations were performed using an available boundary-layer code referred to here as the "spin code." The computations solve a finite-difference set of parabolic boundary-layer equations implicitly in $Y$ and marching in $X$.[12] The program can incorporate different turbulence models ranging from a simple, mixing-length model to a more complicated Reynolds stress equation (RSE) model. Earlier calculations by Higuchi and Rubesin[8] indicated that the Reynolds stress model resulted in better agreement with experiments than did the eddy-viscosity models. Therefore, the computations shown herein were done with the Reynolds stress model.

The RSE model used herein was based on the closure equations of Launder et al.,[13] but with length scale established with the specific dissipation rate $\omega$ ($\omega = \epsilon/0.9k$).[14] The near-wall region is treated with unique damping models consistent with those of Ref. 14.

The computations began at 0.1 boundary-layer thickness upstream of the junction with experimentally measured values of mean velocities and all six Reynolds stresses using a starting procedure developed by Rubesin et al.[15] Starting the calculations with experimental data ensures that downstream differences between the calculations and experiment are caused by the model assumptions and not the initial conditions.

## Results and Discussion

The flowfield was surveyed with (13) profiles so that mean and turbulence quantities could be differentiated in streamwise, as well as normal, directions. The data shown are only a fraction of what were actually used in the analyses. Derivatives were obtained by making piecewise least-square curve fits (quadratic and cubic) to the data. Uncertainties in differentiated quantities are determined by an $n$th order uncertainty analysis and are indicated by error bars on the figures.

The key to understanding this flow is realizing the existence of at least two distinct and different zones: 1) an interaction zone where the fluid responds to the new boundary condition (cessation of spin), and 2) an undisturbed, outer, boundary-layer zone where the flow continues in equilibrium. Figure 1 shows the approximate edge of the interaction zone as implied by the measurements.

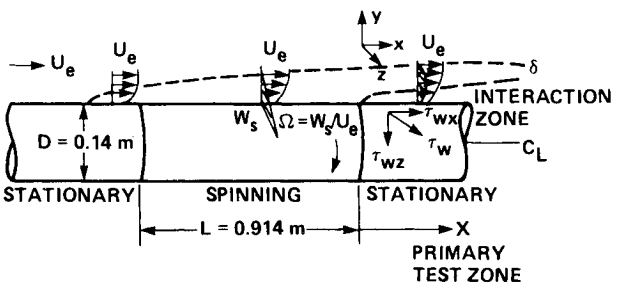


**Fig. 1 Test configuration and flow conditions. $U_e = W_s = 36.3$ m/s, $\delta_0 = 2.9$ cm ($x = 0$).**

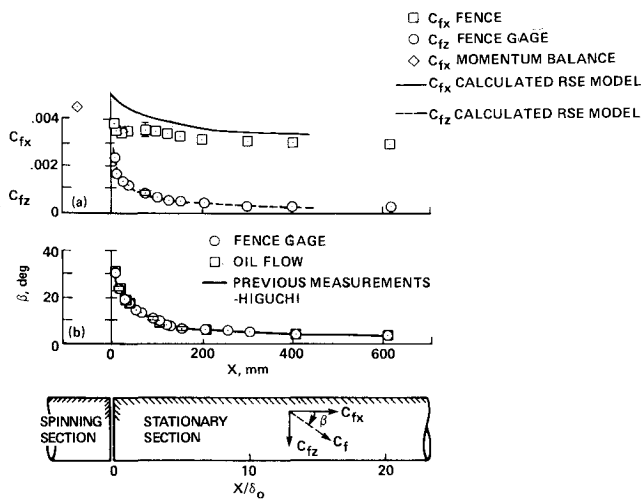


Fig. 2 Skin-friction and surface-flow angle distribution.

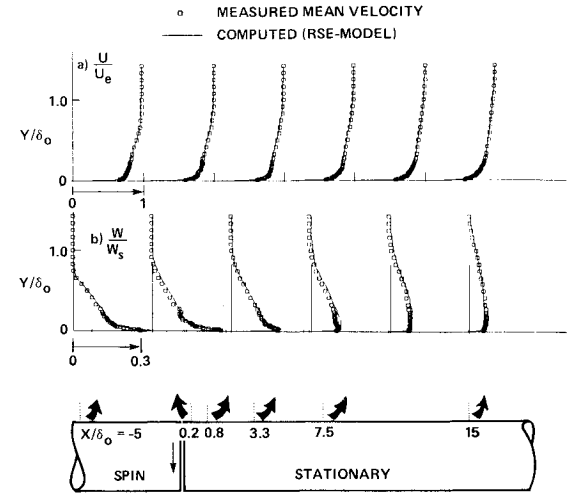


Fig. 3 Mean-velocity measurements and calculations.

### Skin Friction and Surface Streamlines

Skin-friction distribution and surface-flow angle, as measured by the surface fence gage, are shown in Fig. 2. The axial skin friction is about 6% lower than earlier measurements by Higuchi and Rubesin,[8] probably because of a slightly thicker boundary layer in this study (inlet rebuilt between studies). The transverse skin friction agreed very well with the measurements of Ref. 8. As noted in Ref. 8, the transverse-wall shear stress decays exponentially while the axial-wall shear stress decays slowly and similarly to that of a two-dimensional boundary layer. Surface-flow-angle distribution, as measured by the fence gage and surface-oil-flow patterns, can be seen in Fig. 2b. These measured angles compare very well with angles previously measured by Higuchi and Rubesin.[8] Downstream, the surface flow, which was initially 90 deg (i.e., strongly skewed), to nearly 0 deg (two-dimensional). Calculations of skin friction with the RSE model (Fig. 2a) agreed well with the measured values, although the axial component appears overpredicted, probably due to modeling deficiencies.

### Flowfield Measurements

Mean and fluctuating flowfield measurements were made with the three-component LDV. A few profiles of time-averaged $U$ and $W$ velocities are shown in Figs. 3a and 3b, respectively. The symbol size represents a conservative estimate of the experimental uncertainty. Strong cross-flow ($W$) velocities can be seen upstream of the junction on the spinning cylinder (Fig. 3b). Nearest the wall, at $Y^+ = 40$, the $W$ velocity is only 33% of its wall value, indicating that most of the turning is done below $Y^+ = 40$. Downstream of the junction, the transverse component of velocity quickly decays nearest the wall, while away from the wall transverse velocity continues to be unaffected. The streamwise component of velocity ($U$), for the most part, continues unchanged except near the wall where the small accelerations can be seen (Fig. 3a). Calculations of the mean velocities compare well with the measured values, although the $W$ component of velocity has its maximum slightly farther out in the flow than that measured experimentally.

A polar velocity plot ($W$ vs $U$), shown in Fig. 4, reveals the near-equilibrium condition of the boundary layer at the end of spin characterized by the collateral condition ($1 = U/U_e + W/W_s$). This is a desirable initial condition, indicative of nearly zero streamwise derivatives. Downstream of spin, the velocities in the $U$ vs $W$ plane develop the familiar triangular shape. The apex of the triangle decreases with distance downstream. Near the wall, on the slow-speed side of the triangle, velocities extrapolate to zero with the same slope as the measured surface-flow angle, representing a region of nearly constant-flow angle. The outer part of the boundary layer (beyond the local maximum in $W$ velocity) remains undisturbed by the relaxation process.

Measurements of axial shear stress ($\overline{uv}$) are shown in Fig. 5a. These measured values compare reasonably well with stress, as inferred from integrating the mean $X$-momentum equation (using $C_f$ at the wall as a starting point). Nonzero stress at the edge of the boundary layer by the inferred method can be attributed to accumulation of differentiation uncertainties. Differences near the wall reflect inaccuracies in the measurement technique, as discussed in the Appendix. This stress develops similar to that of a two-dimensional boundary layer, with one exception: the measurements reveal a local minimum in shear stress in the inner portion of the boundary layer, indicating a region of flow acceleration. Calculations with the RSE model generally overpredict the shear, showing a sharp maximum near the wall where the data has a minimum. This may explain why skin friction is overpredicted.

Transverse shear stress ($\overline{vw}$), shown in Fig. 5b, initially behaves similarly to axial shear stress ($\overline{uv}$); this is an expected characteristic of collateral flow. Yet, downstream of the junction the transverse shear reverses sign near the wall, responding to the direction reversal of the transverse skin friction. The interaction region ($d\overline{vw}/dy > 0$ for the inner boundary layer) is seen to grow with distance in $X$. Further downstream, this component of shear stress decays as the boundary layer relaxes back to a two-dimensional flow. Also shown are the stresses as inferred from integrating the differential transverse momentum equation. The good agreement between the two measures of shear stress demonstrate the high level of self-consistency of the data. Calculations (also shown) agree extremely well.

Profiles of kinetic energy [$k = (\overline{u^2} + \overline{v^2} + \overline{w^2})/2$], shown in Fig. 6a, exhibit a boundary-layer shape with high levels of kinetic energy near the wall where turbulence is predominantly produced. Downstream of the junction, the kinetic energy decays to a lower level; this is a result of reduced production (removal of production caused by spin). Calculations using the RSE model compare very well in the outer part of the boundary layer, but closer to the wall computed kinetic energy is seen to decay to values lower than those observed experimentally.

Figure 6b shows measured values of the turbulent, triple-product correlation $\overline{vk}$ [$\overline{vk} = (\overline{vu^2} + \overline{v^3} + \overline{vw^2})/2$]. This correlation is a measure of the turbulent diffusion of kinetic energy in the $y$ direction. A positive sign indicates that turbulent mixing is carrying $k$ away from the wall, while

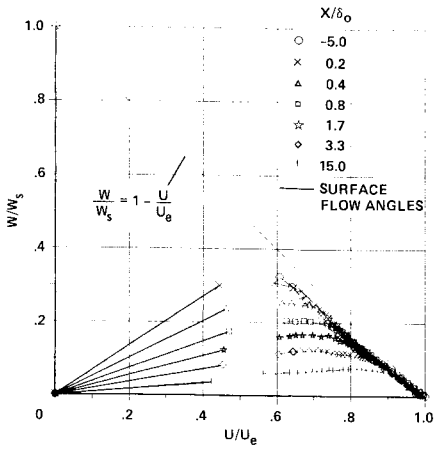


Fig. 4 Polar velocity profile.

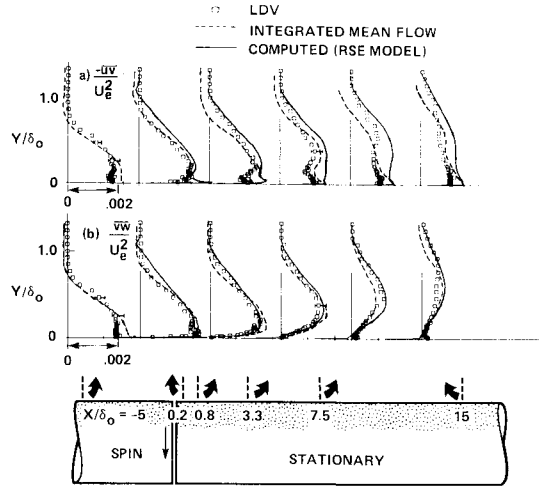


Fig. 5 Reynolds shear-stress profiles ($\overline{uv}$ and $\overline{vw}$) measured and calculated.

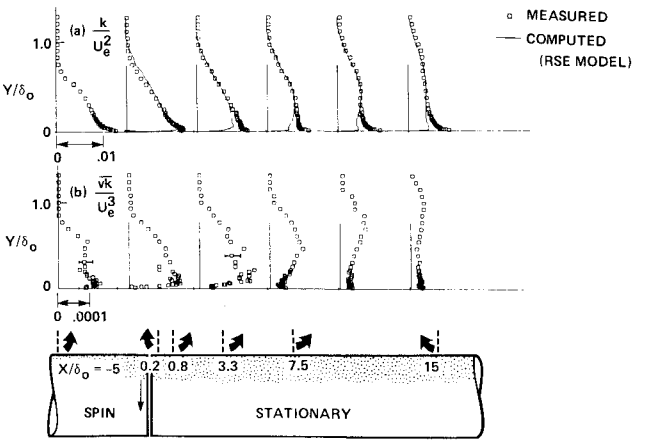


Fig. 6 Kinetic energy and $\overline{vk}$ triple-product profiles.

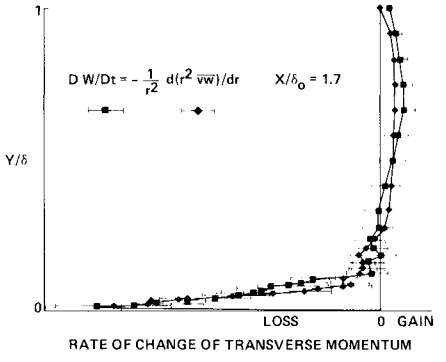


Fig. 7 Transverse momentum equation.

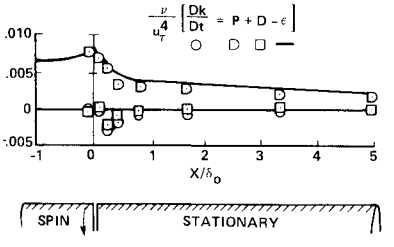


Fig. 8 Kinetic-energy balance along a streamline at $y/\delta_0 = 0.025$.

negative means transport toward the wall. Consistent with the gradient diffusion turbulence model assumption, $\overline{vk}$ is largest where gradients of $k$ are most severe. All ten turbulent triple products were measured (although not shown), and their behavior is similar to that of the $\overline{vk}$ triple product.

An estimate of terms in the transverse momentum equation are shown in Fig. 7 for a station $X/\delta_0 = 1.7$. The measured rate of change of transverse momentum is seen to nearly equal the forces produced by turbulent Reynolds stress. Other forces resulting from normal stresses and molecular viscosity are negligible, and are not shown here. The figure shows that cross-flow momentum near the wall is lost because of frictional forces resisting the flow. Conversely, in the outer part of the boundary layer, the cross-flow continues to accelerate as a result of residual shear-stress forces pulling the fluid in the direction of rotation. This balance demonstrates the high level of self-consistency and differentiability of the data and provides confidence for balancing other turbulent transport equations.

Terms in the transport equation for turbulent kinetic energy are estimated using derivatives of the data (see Fig. 8). Convection, production, and diffusion of kinetic energy are calculated directly, while dissipation is inferred from the balance of the equation (symbol size indicative of uncertainty). Upstream, where the boundary layer is in equilibrium, production nearly equals dissipation; and convective and turbulent transport of kinetic energy are negligible. Downstream, after the initial perturbation at the junction, production of kinetic energy decays to a lower level (a result of losing production due to spin). Dissipation persists at its high level before eventually decaying to a level equal to production. This imbalance in production and dissipation causes a decay of kinetic energy (negative convection). Negative turbulent diffusion indicates a net transport (out-flow) of kinetic energy from local regions of high concentration to neighboring regions of low concentration. Figure 8 reveals the tendency of dissipation to lag behind production.

## Turbulence Model Testing

Until now, the discussion has focused on the physical behavior of the flow. We now turn our attention to the testing and evaluation of various turbulence modeling assumptions. In an effort to test each model individually, we directly substitute experimental measurements into the right-hand side of the model and compare the result with the experimentally measured left-hand side. No computational results are used here; the analysis is done strictly with data.

One such turbulence modeling assumption involves the notion of eddy viscosity. This idea, borrowed from laminar fluid flow, states that stress on an element of fluid is propor-

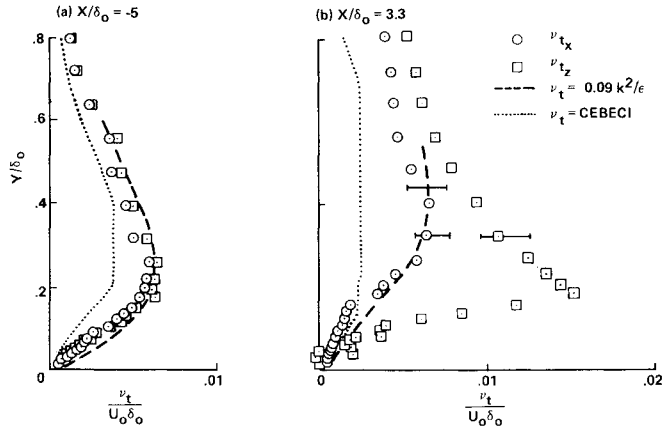


Fig. 9 Turbulent eddy-viscosity components $\nu_{t_x}$ and $\nu_{t_z}$.

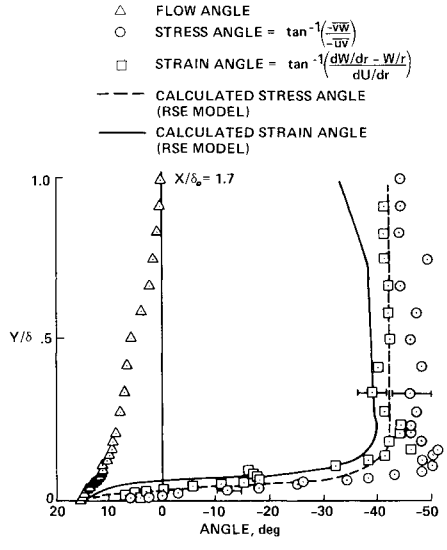


Fig. 10 Profile of principal stress and strain angles at $X/\delta_0 = 1.7$.

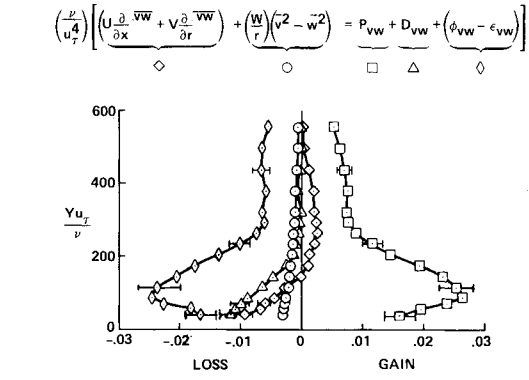


Fig. 11 Transport equation for $\overline{vw}$ Reynolds shear stress at $X/\delta_0 = 0.2$.

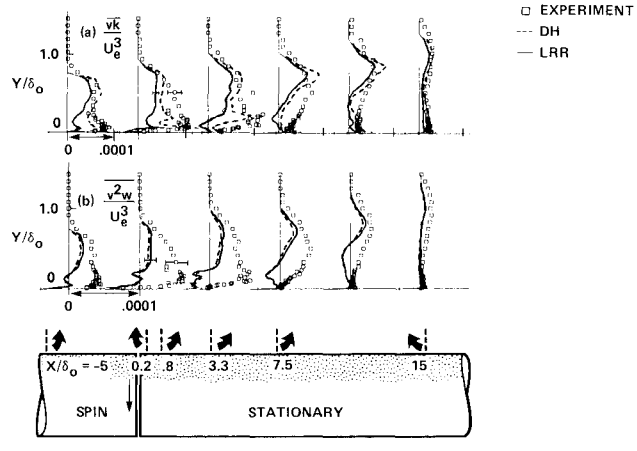


Fig. 12 Turbulent diffusion models for $\overline{vk}$ and $\overline{v^2w}$.

tional to the strain rate (by a constant of proportionality $\nu_m$). Similarly, in turbulent flow the Reynolds stress is often assumed to be proportional to the mean-flow strain rate (by a constant of proportionality, $\nu_t$) as follows:

$$-\overline{uv} = \nu_{t_x}\frac{\partial U}{\partial r}$$

$$-\overline{vw} = \nu_{t_z}\left(\frac{\partial W}{\partial r} - \frac{W}{r}\right)$$

where $\nu_{t_x}$ and $\nu_{t_z}$ are prescribed by a turbulence model. Many models assume (prescribe) that eddy viscosity is a scalar independent of direction ($\nu_{t_x} = \nu_{t_z}$), thus simplifying computations. To check this assumption, components of eddy viscosity were determined from the data (using the preceding relationships) at locations $-5\delta_0$ upstream and $+3.3\delta_0$ downstream of the junction (see Fig. 9). At the upstream station, both components of eddy viscosity are virtually equal to each other (isotropic condition). At the downstream station, the viscosities differ by a factor of 3 or 4. This illustrates the nonisotropic nature of eddy viscosity and indicates the need for a full Reynolds stress turbulence model. Also shown are two prominent models for scalar eddy viscosity. The Jones-Launder[16] model ($\nu_{t_x} = \nu_{t_z} = 0.09\, k^2/\epsilon$) works quite well for modeling the $\nu_{t_x}$ component of eddy viscosity, while the Cebeci[17] model

$$\nu_{t_x} = \nu_{t_z} = 0.0168\int_0^{\delta}(1+y/r)\,[Q_e - Q(y)]\,dy \div [1+5.5(y/\delta)^6] \quad \text{outer layer}$$

$$= (0.4y)^2\frac{\partial Q}{\partial y} \quad \text{inner layer}$$

rather severely underpredicts $\nu_{t_x}$. Neither is capable of simulating $\nu_{t_z}$.

The direction-dependency of eddy viscosity can be understood by look at the direction of the principal strain and stress vectors (see Fig. 10 for location $X = 1.7\delta_0$). In the outer portion of the boundary layer, stress is observed to be nearly aligned with the strain (45 deg). Nearer the wall, in the interaction region, the stress and strain turn toward the flow angle. Here the stress and strain angles are different (nonaligned) by as much as 25 deg. It appears that the disturbance to mean flow strain diffuses farther into the boundary layer than does the disturbance to stress. Physically, the disturbance to stress lags behind the disturbance to the mean flow strain. In other words, the mean flow responds to the sudden change in wall boundary condition before the turbulence does. This phenomenon has been observed by others.[1] This nonalignment of stress and strain points to a need for an anisotropy model, such as full Reynolds stress modeling. Also shown are calculations using the RSE model, which demonstrates the model's ability to produce stress in a different direction than the mean-flow strain rate.

Full RSE models are gaining wider popularity with an increasing desire to compute more complex flows. The RSE model's popularity stems from its ability to predict the anisotropy of Reynolds stresses which exists in complex flows. By solving a set of equations that govern the transport of individual Reynolds stresses, there is more freedom to allow for anisotropic behavior. Derivation of the transport equation for Reynolds shear stress $\overline{vw}$, in cylindrical coordinates, results in

$$U\frac{\partial \overline{vw}}{\partial x}+V\frac{\partial \overline{vw}}{\partial y}+(\overline{v^2}-\overline{w^2})W/r$$

Convection ($C_{vw}$)

$$=\left[-\frac{\partial(r\overline{v^2w})}{\partial r}-(\overline{v^2w}-\overline{w^3})\right]\Big/r$$

Diffusion ($D_{vw}$)

$$+\left(-\overline{v^2}\frac{\partial W}{\partial r}+\overline{w^2}W/r\right)+\phi_{vw}-\epsilon_{vw}$$

Production ($P_{vw}$) Pressure strain Dissipation

where $\phi_{vw}$ and $\epsilon_{vw}$ are symbolic representations for the terms commonly called the pressure rate-of-strain and dissipation. The only terms that do not have to be modeled in this equation are the convection and production terms, which are functions of known quantities. Models are required for diffusion, pressure strain, and dissipation. Experimentally, convection, diffusion, and production can be obtained from the data, and the sum $\phi_{vw}-\epsilon_{vw}$ can be inferred by balance of the equation. Measurements of terms in this equation and inferred $\phi_{vw}-\epsilon_{vw}$ (by balance) are shown in Fig. 11 for a location $X/\delta_0=0.2$. Production and pressure strain (plus dissipation) are the dominant terms in the equation, with diffusion and curvature terms some what smaller, and convection smaller yet. The relatively small magnitude of the convective term is a concern to turbulence model inventors, since solving for this term requires extreme accuracy in modeling the other terms.

Models for the diffusion term have been suggested by Daly and Harlow (DH)[18] and Launder, Reece, and Rodi (LRR).[13] The DH model for the diffusion term is

$$-\overline{u_iu_ju_k}=C_s'(k/\epsilon)\overline{u_ku_l}\frac{\partial \overline{u_iu_j}}{\partial x_l}$$

and the LRR model is

$$-\overline{u_iu_ju_k}=C_s(k/\epsilon)\left[\overline{u_iu_l}\frac{\partial \overline{u_ju_k}}{\partial x_l}+\overline{u_ju_l}\frac{\partial \overline{u_ku_i}}{\partial x_l}+\overline{u_ku_l}\frac{\partial \overline{u_iu_j}}{\partial x_l}\right]$$

where $C_s'=0.25$ and $C_s=0.11$.

Both models have a similar form, but the latter has the advantage that it is invarient under permutation of indices. Measurements of the triple-product correlation $\overline{vk}$ and $\overline{v^2w}$ are compared with these model assumptions in Fig. 12. The models are evaluated using experimentally measured $\overline{v^2}$, $\overline{vw}$, $k$, and $\epsilon$ as inputs. Both models for $\overline{vk}$ are similar in shape to the measured values, with the simpler DH model being perhaps somewhat more accurate. As for modeling the $\overline{v^2w}$ triple product, neither model works particularly well, but it is encouraging to see that the functional forms of both models are somewhat similar to that of the data.

Models for the pressure rate-of-strain and dissipation terms ($\phi_{vw}-\epsilon_{vw}$) have been suggested by Naot, Shavit, and Wolfshtein (NSW)[19] and LRR.[13]

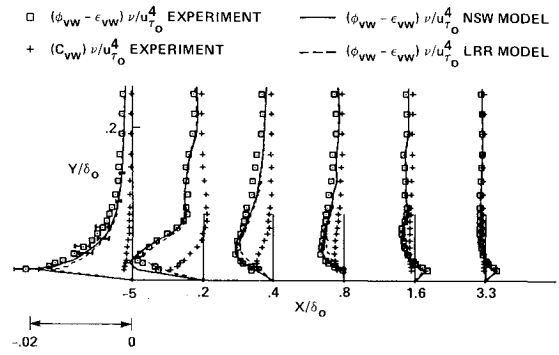


**Fig. 13 Pressure rate-of-strain turbulence models.**

$$\phi_{vw}=-\gamma\left[-\overline{v^2}\frac{\partial W}{\partial y}+\overline{w^2}W/r\right]-C_1(\epsilon/k)\overline{vw} \qquad \text{(NSW)}$$

$$=-C_4\left[-\overline{v^2}\frac{\partial W}{\partial r}+\overline{w^2}W/r\right]-C_5k\left(\frac{\partial W}{\partial r}-W/r\right)$$

$$-C_6\left[-\overline{uw}\frac{\partial U}{\partial r}-\overline{w^2}\frac{\partial W}{\partial r}+\overline{v^2}W/r\right]-C_1(\epsilon/k)\overline{vw}$$

$$+\left\{0.125(\epsilon/k)\overline{vw}+0.015\left[(w^2-v^2)\left(\frac{\partial W}{\partial r}-W/r\right)+\overline{uw}\frac{\partial U}{\partial r}\right]\right\}(k^{1.5})/(\epsilon y) \qquad \text{(LRR)}$$

$$\epsilon_{vw}=0 \qquad \text{(NSW and LRR)}$$

where $\gamma=0.6$, $C_1=1.5$, $C_4=0.764$, $C_5=0.182$, and $C_6=0.109$.

Both models for $\phi_{vw}-\epsilon_{vw}$ are calculated by plugging experimental data into the right-hand side of the preceding relationships. Experimentally inferred $\phi_{vw}-\epsilon_{vw}$ is compared with these model assumptions in Fig. 13. Both models seem to do remarkably well, considering they had very little guidance from experimental data. Nevertheless, differences are seen in regions where the flow's three-dimensionality is strongest. These differences appear large in comparison to the relatively small convection term (also shown) for which the Reynolds stress transport equation is solved. Experimental uncertainties can account for some of the differences, making it difficult to determine which model works best.

## Conclusions

New turbulence measurements using a three-component laser Doppler velocimeter (LDV) were compared with differential-momentum balances. While some deficiencies were noted in the LDV measurements, the level of accuracy was high.

The relaxation of a three-dimensional shear-driven turbulent boundary layer to a two-dimensional layer was experimentally studied with the three-component LDV in an effort to better understand and model the turbulent transport processes. Flow initially swirling about a spinning cylinder passes over a stationary section of the cylinder and produces a sudden change in boundary conditions. The perturbation (change in boundary condition) diffuses into the initial turbulent boundary layer with a secondary boundary-layer-type growth. The perturbation effect is not instantly felt throughout the boundary layer. This perturbed region of the boundary layer produces fairly strong anisotropies in the eddy viscosities (Reynolds stress). Full Reynolds stress transport equation models predict this anisotropy to some

extent. In both the experiment and the full Reynolds stress model calculations, the Reynolds shear-stress response to the change in boundary condition lags the response of the mean flowfield. The rate equations governing the evolution of Reynolds stress demonstrate the small relative size of the convection term compared to production, diffusion, pressure-strain, and dissipation terms.

Turbulence models were tested using the date. Models for turbulent triple products were comparable to the experimentally measured triple products, although there is room for improved accuracy. Models for the pressure rate of strain also compared well to experimentally deduced pressure strain, although the small differences were large relative to the small convection term. Calculations using a Reynolds stress equation turbulence model generally agreed well with the data.

## Appendix

Several researchers have recently developed three-component LDV systems.[20-24] These efforts have been primarily focused on obtaining mean velocities, without concern about turbulence measurements. While attempts have been made to measure turbulence quantities, very few results have actually been reported and those that have been reported were done in complex flows for which there is little or no means for comparison. Recently, Bell et al.[24] compared their three-component LDV measurements directly with a cross wire. The LDV and hot-wire data compared to within 10-20% on all measurements except $\overline{uw}$, which was different by 50% ($\overline{vw}$ was not compared). The work presented here is concerned with the measurement of turbulence quantities and uncertainties associated with these quantities.

### LDV Configuration

The system (shown in Fig. A1) uses three different color beam pairs (forward scatter), all intersecting (nearly orthogonal) at the same point in space. Only simultaneous measurements of all three velocities are collected. Then each velocity triplet is transformed into Cartesian velocity components and ensemble averages are performed.

An argon ion laser generated blue (488 nm) and green (514.5 nm) beam sets which measured $V-0.0221U+0.0043W$ (small dip angle) and $0.883U-0.470W$ ($-28.05$-deg direction) components of velocity, respectively. A second argon ion laser generated a violet (476.5 nm) pair of beams, which measured a $0.872U+0.489W$ ($+29.3$-deg direction) component of velocity. Fringe spacings were 9.090, 8.711, and 3.326 $\mu$m for the green, blue, and violet beams, respectively. Bragg shifting (40 MHz) was applied to each of the three pairs of beams.

Electronic signal processing was performed with two TSI counters and one in-house-designed counter (ARC-1). Resolution of the TSI counters and the ARC-1 counter was $\pm 1.0$ and $\pm 0.8$ ns, respectively. Sixteen fringes were counted. A logic circuit built at the NASA Ames Research Center was used to validate only velocity measurements received simultaneously ($\pm 5$ $\mu$s). At each measuring station, 10,000 velocity triplets were collected for use in ensemble averaging. The flow was seeded with 0.5-$\mu$m diam latex particles.

A potential source of error exists: multiple seeds in the measuring volume. Most of the time, one particle is in the scattering volume at a time and, occasionally, it is at the intersections of all three volumes. Infrequently, one particle is in one volume and another particle is simultaneously in the other volume. These particles will be counted and validated, even though the velocity components are measured at different locations. This can cause errors in measuring fluctuating quantities, if the turbulence scale is smaller than the distance between the particles. Multiple seed particle measurements (occurring a small percentage of the time) are thought to be systematically causing lower values of 10-20% in the $\overline{uv}$ and $\overline{vw}$ shear stresses.

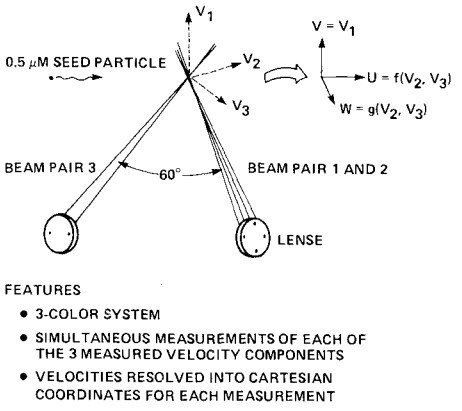


**Fig. A1 Three-component LDV configuration.**

## Acknowledgments

The authors are grateful to H. L. Seegmiller and A. DeYoung for their initial design of the three-component LDV system and for their helpful suggestions during this study. Thanks also to Drs. M. Rubesin and J. Viegas for instructions on how to use the spin code and for making some useful modifications to it. The authors would like to express sincere thanks to Drs. J. G. Marvin and M. Rubesin for their encouragement and suggestions during the investigation. This research was conducted while the second author held a Senior National Research Council Research Associateship at the NASA Ames Research Center.

## References

[1]Johnston, J. P., "Experimental Studies in Three Dimensional Turbulent Boundary Layers," Thermosciences Division, Department of Mechanical Engineering, Stanford University, Stanford, CA, Rept. MD-34, July 1976.

[2]Elsenaar, A. and Boelsma, S., "Measurements of the Reynolds Stress Tensor in a Three-Dimensional Turbulent Boundary Layer Under Infinite Swept-Wing Conditions," National Aerospace Laboratory, the Netherlands, NLR TR 74095 U, 1974.

[3]Müller, U., "Measurements of the Reynolds Stresses and the Mean Flow Field in a Three-Dimensional Pressure Driven Boundary Layer," *Journal of Fluid Mechanics*, Vol. 119, pp. 121-153.

[4]Pontikos, N. and Bradshaw, P., "The Structure of Three-Dimensional Turbulent Boundary Layers," Ph.D. Thesis, Department of Aeronautics, Imperial College, London, England, Sept. 1982.

[5]Furuya, Y., Nakamura, I., and Kawachi, H., "The Experiment on the Skewed Boundary Layer on a Rotating Body," *Bulletin of the Japan Society of Mechanical Engineers*, Vol. 9, 1966, p. 702.

[6]Bissonnette, L. R and Mellor, G. L., "Experiments on the Behavior of an Axisymmetric Turbulent Boundary Layer with a Sudden Circumferential Strain," *Journal of Fluid Mechanics*, Vol. 63, Pt. 2, April 1974, pp. 369-413.

[7]Lohmann, R., "The Response of a Developed Turbulent Boundary Layer to Local Transverse Surface Motion," *Transactions of ASME, Journal of Fluids Engineering*, Vol. 98, Sept. 1976, pp. 354-363.

[8]Higuchi, H. and Rubesin, M. W., "An Experimental and Computational Investigation of the Transport of Reynolds Stress in an Axisymmetric Swirling Boundary Layer," AIAA Paper 81-0416, Jan. 1981.

[9]Higuchi, H. and Rubesin, M. W., "Behavior of a Turbulent Boundary Layer Subjected to Sudden Transverse Strain," *AIAA Journal*, Vol. 17, Sept. 1979, pp. 931-941.

[10]Nakamura, I. and Yamashita, S., "Boundary Layers on Bodies of Revolution Spinning in Axial Flows," *IUTAM Symposium on Three-Dimensional Turbulent Boundary Layers*, Berlin, FRG, March 1982.

[11]Driver, D. M. and Hebbar, S. K., "Experimental Study of a Three-Dimensional, Shear-Driven, Turbulent Boundary Layer Using a Three-Dimensional Laser Doppler Velocimeter," AIAA Paper 85-1610, July 1985.

[12]Wilcox, D. C., "Recent Improvements to the Spinning Body Version of the EDDYBL Computer Program," DCW Industries Inc.,, Studio City, CA, Rept. DCW-R-24-01, Nov. 1979.

[13]Launder, B. E., Reece, G. J., and Rodi, W., "Progress in the Development of a Reynolds-Stress Turbulence Closure," *Journal of Fluid Mechanics*, Vol. 68, Pt. 3, 1975, pp. 537-566.

[14]Wilcox, D. C. and Rubesin, M. W., "Progress in Turbulence Modeling for Complex Flow Fields Including Effects of Compressibility," NASA TP 1517, April 1980.

[15]Rubesin, M. W., Higuchi, H., Olsen, M. E., and Viegas, J. R., "A Reexamiantion of the Behavior of a Transversely Shear-Strained Turbulent Boundary Layer," NASA TM (to appear).

[16]Jones, W. P. and Launder, B. E., "The Prediction of Laminarization with a Two-Equation Model of Turbulence," *International Journal of Heat and Mass Transfer*, Vol. 15, Feb. 1972, pp. 301-304.

[17]Cebeci, T., "Calculation of Three-Dimensional Boundary Layers I. Swept Infinite Cylinders and Small Cross Flow," *AIAA Journal*, Vol. 12, June 1974, pp. 779-786.

[18]Daly, B. and Harlow, F., "Transport Equations in Turbulence," *The Physics of Fluids*, Vol. 13, Nov. 1970, pp. 2634-2649.

[19]Naot, D., Shavit, A., and Wolfshtein, M., "Two-Point Correlation Model and the Redistribution of Reynolds Stresses," *The Physics of Fluids*, Vol. 16, June 1973, pp. 738-743.

[20]Yanta, W. J., "A Three-Dimensional Laser Doppler Velocimeter for Use in Wind Tunnels," *International Congress on Instrumentation in Aerospace Simulation Facilities,* Monterey, CA, Sept. 1979 (IEEE Pub. 79CH 1500-8 AES).

[21]Ausherman, D. W. and Yanta, W. J., "The Three-Dimensional Turbulent Transport Properties in the Boundary Layers of Conical Body Configurations at Mach 3," AIAA Paper 84-1528, June 1984.

[22]Meyers, J. F., *Proceedings—International Symposium on Applications of Laser Doppler Anemometry to Fluid Mechanics*, Lisbon, Portugal, July 1982.

[23]Orloff, K. L. and Snyder, P. K., "Laser Velocimetry in the Low-Speed Wind Tunnels at Ames Research Center," NASA TM-85855, 1984.

[24]Bell J., Rodman, L., and Mehta, R., "Aspects of the Design and Performance of a Three-Component LDV System," 11th ICIASF Meeting on Instrumentation, Stanford Univ., Stanford, CA, Aug. 1985.